JACS
JOURNAL OF THE AMERICAN CHEMICAL SOCIETY
pubs.acs.org/JACS
Article

Identification of Highly Active Co−O−Zn Sites in Silanol Nests for *n*-Butane Cascade Dehydrogenation to 1,3-Butadiene

Yanfei Zhang,* Tingshu Yang, Jiaochan Hu, Linying Wang, Mingbin Gao,* Liang Qi, Alexis T. Bell,* Peng Tian,* and Zhongmin Liu

Cite This: *J. Am. Chem. Soc.* 2025, 147, 42110−42122

ABSTRACT: *n*-Butane dehydrogenation (BDH) provides an on-purpose route to produce 1,3-BD. However, design of highly active and selective catalysts targeting BDH to 1,3-BD remains challenging because the activation barrier for the dehydrogenation of 1-butene (a primary product of BDH) is high and 1-butene readily isomerizes. Here, we report a bimetallic Co−O−Zn active site with the structure of ≡SiO−Co−O−Zn−OSi≡ prepared by reacting Co ions with ≡SiOZn−OH nests on dealuminated zeolite BEA (DeAlBEA), showing 3- and 34-fold activity advantages over monometallic Co and Zn counterparts, respectively. Co−O−Zn sites exhibit a high BDH rate of 354 $mol \cdot mol_{Co}^{-1} \cdot h^{-1}$ and a 1,3-BD productivity of 110 $mol \cdot mol_{Co}^{-1} \cdot h^{-1}$ (and selectivity to 1,3-BD of 31%) at 823 K. The forward rate coefficient for BDH is superior to state-of-the-art non-noble-metal catalysts and comparable to Pt-based catalysts. A kinetics investigation suggests that the Co−O−Zn interactions promote *n*-butane adsorption and activation of the C−H bond during both BDH and 1-butene dehydrogenation. Our work demonstrates a promising pathway for producing 1,3-BD via BDH using a catalyst that is free of expensive noble metals.

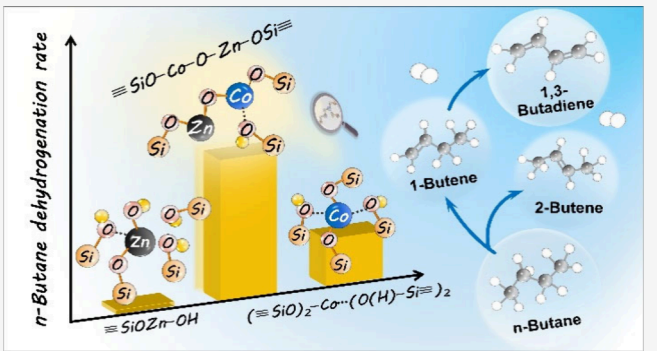

1. INTRODUCTION

1,3-Butadiene (1,3-BD) is widely used to produce high value-added polymers such as acrylonitrile−butadiene−styrene (ABS) and styrene−butadiene rubber (SBR) with its global market value reaching USD 42.3 billion in 2024.[1,2] Traditionally, 95% of 1,3-BD has been obtained as a byproduct of naphtha steam cracking, used primarily to produce ethene.[3] Due to the recent availability of low-cost light ethane present in shale gas, the production of ethene has shifted from petroleum cracking and steam reforming of naphtha to thermal dehydrogenation of ethane, resulting in reduced availability of C_4 distillate needed to produce 1,3-BD.[4−7] For this reason, direct dehydrogenation of naphtha-derived *n*-butane to C_4 olefins has become an attractive option for the on-purpose production of 1,3-BD.

While industrial processes for ethane and propane dehydrogenation, e.g., the Oleflex[8] and Catofin[9] processes, using either a Pt-based or CrO_x-based catalyst, are well established, the development of a selective process for production to 1,3-BD via *n*-butane dehydrogenation (BDH) has yet to be achieved.[10] For example, the Houdry-Catadiene process for BDH, which uses a mixture of CrO_x and Al_2O_3, exhibits a relatively low 1,3-BD selectivity (∼15%),[2] and Pt- and Ir-based catalysts are also selective to butene.[11,12] Catalyst design and reaction mechanistic analysis serve as the fundamental pillars for advancing chemical process industrialization, a pursuit long prioritized by chemical engineers. Consequently, precise construction of an active and selective catalyst for BDH to 1,3-BD, along with elucidating the underlying mechanism and kinetics on them, is highly desirable.

There has been considerable recent interest in exploring cost-effective non-noble-metal-based Lewis acid catalysts for alkane dehydrogenation.[13−24] Isolated Fe sites incorporated into dealuminated BEA (DeAlBEA) comprising single units and clusters of $(-Si-O)_2Fe^{3+}-OH$ are reported to exhibit good propane dehydrogenation activity in the presence of co-fed H_2.[17] And ZnO_x-silicalite-1 containing active sites, formed via a reaction of support hydroxyl groups with Zn atoms generated from ZnO upon reduction, is reported to exhibit about 3-fold higher propene productivity than K-CrO_x/Al_2O_3.[15] However, the activity of BDH over non-noble-

Received: September 17, 2025
Revised: October 17, 2025
Accepted: October 20, 2025
Published: October 29, 2025

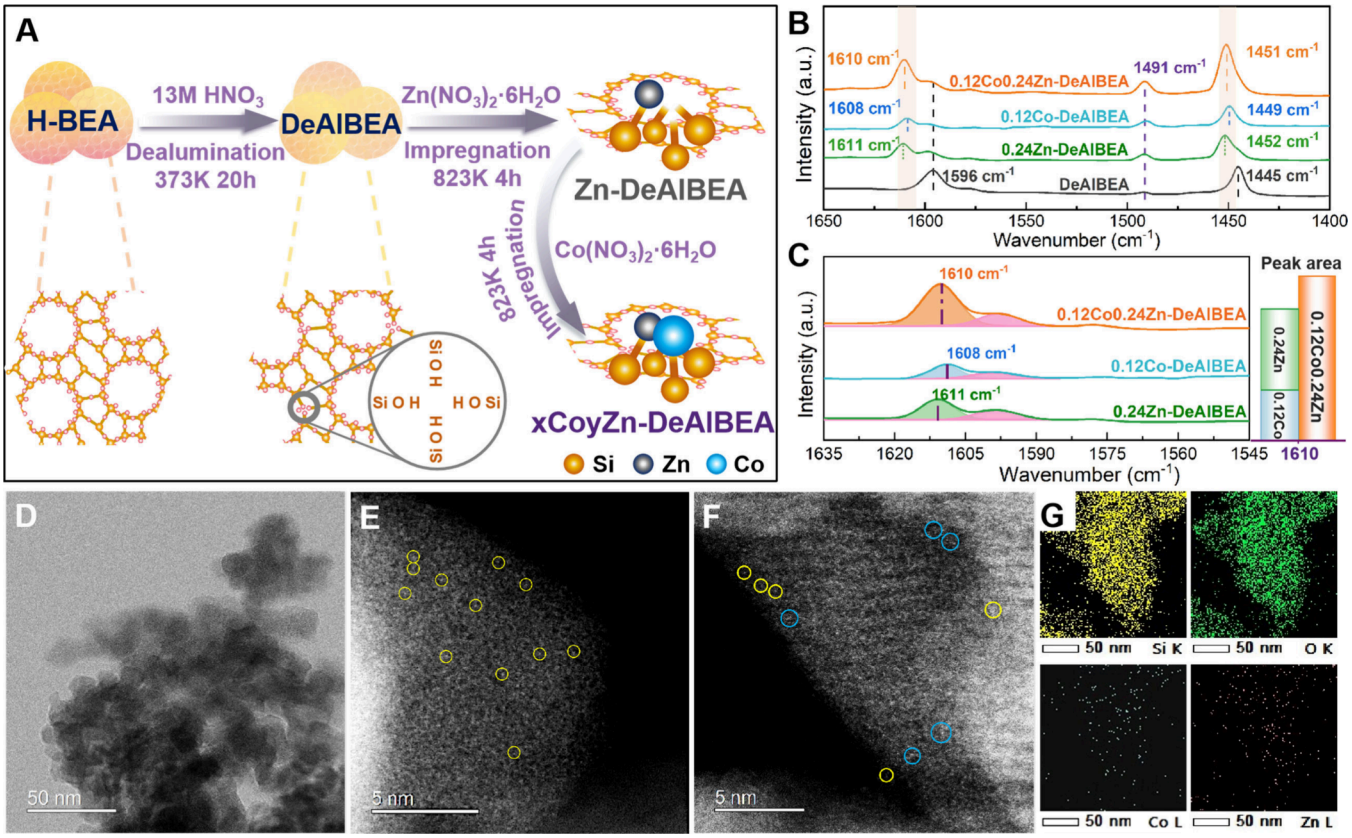

Figure 1. (A) Schematic for the preparation of CoZn-DeAlBEA. (B) IR spectra of adsorbed pyridine on DeAlBEA, 0.24Zn-DeAlBEA, 0.12Co-DeAlBEA, and 0.12Co0.24Zn-DeAlBEA and (C) deconvolution of Lewis acid bands. HAADF-STEM images of (D, E) Co-DeAlBEA and (F) CoZn-DeAlBEA. (G) Energy-dispersive X-ray maps for CoZn-DeAlBEA.

metal-based Lewis acid centers is generally low and the selectivity to 1,3-BD is poor.[13,23,25]

Secondary transition metals (M) such as Sn, Zn, Ga, Fe, and Ce are often employed as promoters for Pt-based catalysts,[26,27] to facilitate dispersion of Pt atoms and modulate their electronic properties, enabling attainment of high alkane dehydrogenation activity.[11,28−33] We have investigated the performance of isolated $(\equiv Si-O-Zn)_{4-6}Pt$ complexes in PtZn-DeAlBEA and PtZn-SPP (self-pillared pentasil) for *n*-butane dehydrogenation and reported that the dehydrogenation activity increased as the coordination number of Pt−Zn bonds decreased from 6 to 4.[34−36] For non-noble-metal-based catalysts, tricoordinate Co atoms, i.e., (≡Si−O)CoO(O−Mo), in Mo-doped Silicalite-1, prepared using organic $[Co(H_2NCH_2CH_2NH_2)_3](NO_3)_2$ as the metal precursor, exhibit a propene formation rate of 22.6 $mol \cdot g_{Co}^{-1} \cdot h^{-1}$ at 823 K, 25.3 kPa propane, and a weight-hourly space velocity of 4.5 h^{-1}, which is nearly an order magnitude higher than that of tetracoordinated Co-based catalysts.[19] To understand the activity of non-noble-metal-based Lewis acid sites on *n*-butane dehydrogenation to 1,3-BD, we have investigated the effect of Zn loading on the mechanism and kinetics of ≡SiOZn−OH sites supported on DeAlBEA.[37] We found that increasing Zn loading enabled the Zn species to undergo a transition from isolated ≡SiOZn−OH sites to nested structures. This change enhanced electron transfer between Zn and oxygen atoms in adjacent ≡SiOZn−OH groups, thereby increasing the dehydrogenation activity of ≡SiOZn−OH nests for converting *n*-butane to butenes. However, the activity of nested ≡SiOZn−OH sites for butene dehydrogenation to 1,3-BD remained identical to that of isolated ≡SiOZn−OH sites, which is attributed to the breakup of the weak interactions between proximal Zn atoms in nested ≡SiOZn−OH groups.

Inspired by the recognition that secondary metal atoms increase site activity, we hypothesized that construction of bimetallic M_1-M_2 or M_1-O-M_2 sites could lead to enhanced dehydrogenation activity for both BDH to butenes and subsequent butene dehydrogenation to 1,3-BD relative to that attainable with monometallic sites. This reasoning was motivated by our recent demonstration that Pt−Zn sites produced by reaction of nested ≡SiOZn−OH sites with Pt form $(\equiv Si-O-Zn)_{4-6}Pt$ sites in DeAlBEA. Compared to Zn-DeAlBEA, the rate of 1,3-BD production over PtZn-DeAlBEA is 270 times higher at 823 K and 2.53 kPa *n*-butane.[34]

Here, we report the preparation of Co−O−Zn bimetallic sites formed by reaction of Co ions with ≡SiOZn−OH nests created in DeAlBEA and investigate this catalyst (CoZn-DeAlBEA) for BDH to form 1,3-BD. The chemical structure of Co active sites in CoZn-DeAlBEA was established to be (≡SiO)−CoOZn−(OSi≡), based upon data from infrared (IR) spectroscopy, X-ray photoelectron spectroscopy (XPS), ultraviolet−visible (UV−vis) spectroscopy, and X-ray absorption spectroscopy (XAS). For comparison, isolated Co sites with tetrahedrally coordination structure of $(\equiv SiO)_2-Co\cdots(O(H)-Si\equiv)_2$ were also prepared within the silanol nests of DeAlBEA. The Co−O−Zn sites exhibit a net rate of BDH of 47.8 $mol \cdot mol_{Co}^{-1} \cdot h^{-1}$ at 723 K, 2.5 kPa *n*-butane, and 7.1 h^{-1}, which is 3 and 34 times higher than that over isolated Co sites and ≡SiOZn−OH nests, respectively. Notably, in sharp contrast to what has been observed for isolated versus nested

https://doi.org/10.1021/jacs.5c16367
J. Am. Chem. Soc. 2025, 147, 42110−42122

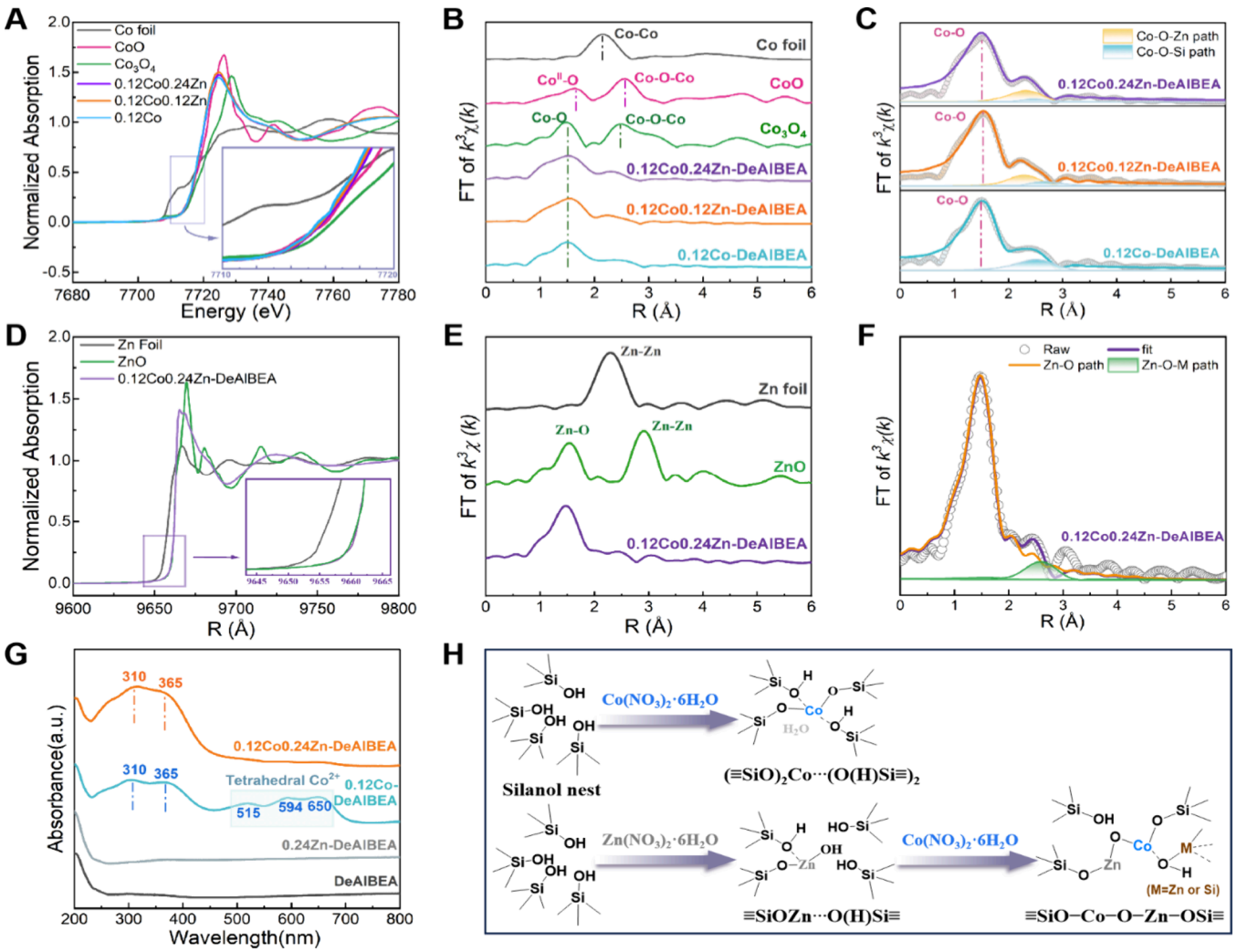

Figure 2. (A) Normalized Co K-edge XANES spectra and (B) FT-EXAFS spectra of Co-DeAlBEA, CoZn-DeAlBEA, and Co standards. (C) Fitting curves of Co K-edge EXAFS spectra for Co-DeAlBEA and CoZn-DeAlBEA. (D) Normalized Zn K-edge XANES spectra and (E) FT-EXAFS spectra of CoZn-DeAlBEA and Zn standards. (F) Fitting curves of Zn K-edge EXAFS spectra for CoZn-DeAlBEA. (G) UV−vis spectra of DeAlBEA, Zn-DeAlBEA, Co-DeAlBEA, and CoZn-DeAlBEA. (H) Schematic illustration of the chemical structure of isolated Co sites and Co−O−Zn sites during synthesis.

≡SiOZn−OH sites, the rates for both *n*-butane dehydrogenation to butene and 1-butene dehydrogenation to 1,3-BD were higher for the Co−O−Zn structure. To identify the reaction mechanism of *n*-butane dehydrogenation and the superior catalytic performance over Co−O−Zn sites, we investigated the kinetics of *n*-butane dehydrogenation to butene isomers and 1-butene dehydrogenation to 1,3-BD over both isolated Co sites and Co−O−Zn sites.

2. RESULTS AND DISCUSSION

2.1. Preparation of Isolated Co Sites and Co−O−Zn Sites. The preparation of isolated Co sites and bimetallic Co−O−Zn sites in the silanol nests of dealuminated BEA zeolite (DeAlBEA) was achieved by wet impregnation and subsequent calcination (Figure 1A). DeAlBEA was obtained by suspending H-BEA (Si/Al = 27) in concentrated nitric acid at 373 K for 20 h to dealuminate.[37] ^{27}Al MAS NMR confirmed the complete removal of Al after dealumination,[36] while the formation of silanol nests at Al-vacancy sites was demonstrated by the appearance of a broad infrared (IR) band centered at around 3500 cm^{-1} (Figure S1A).[37,38] Figure S1B displays the pyridine-adsorbed IR spectra of H-BEA and DeAlBEA. Following dealumination, the IR bands at 1545 cm^{-1} and 1637 cm^{-1} attributable to Brønsted acidic sites, bands at 1455 cm^{-1} and 1620 cm^{-1} corresponding to Lewis acidic sites, and a band at 1490 cm^{-1} corresponding to the combination of both Brønsted and Lewis acidic sites vanished.[39] In place of those IR bands, bands at 1447 cm^{-1} and 1598 cm^{-1} became prominent for DeAlBEA, evidencing the removal of Al from H-BEA and formation of hydrogen (H)-bonded silanol nests.[40] Contacting DeAlBEA with controlled amounts of $Zn^{2+}(OH)_x(H_2O)_{6-x}$ cations or $Co^{2+}(OH)_x(H_2O)_{6-x}$ cations resulted in the formation of Si−O−M bonds to form Zn-DeAlBEA and Co-DeAlBEA.

IR characterization of Zn-DeAlBEA shows that the intensity of the hydroxyl (−OH) band attributable to silanol nests decreases remarkably after Zn incorporation, indicating the grafting of Zn species into the silanol nests of DeAlBEA to form Si−O−Zn bonds.[37] Characterization by XAS, UV−vis spectroscopy, XPS, and IR spectroscopy of adsorbed pyridine and 2,6-di-*tert*-butylpyridine suggests that Zn species are present as isolated ≡SiOZn−OH sites for a Zn/Al ratio

https://doi.org/10.1021/jacs.5c16367
J. Am. Chem. Soc. 2025, 147, 42110−42122

below 0.12, while ≡SiOZn−OH sites form nests for a Zn/Al ratio between 0.12 and 0.60 in which a H-bonding interaction between adjacent Zn−OH groups occurs.[37]

CoZn-DeAlBEA was prepared by reaction of $Co^{2+}(OH)_x(H_2O)_{6-x}$ cations with ≡SiOZn−OH nests in Zn-DeAlBEA. The X-ray diffraction (XRD) patterns of DeAlBEA and metal-supported DeAlBEA exhibit characteristic peaks of BEA zeolite and the absence of peaks for bulk CoO_x or ZnO_x, indicating the high dispersion of metal species in the BEA zeolitic matrix (Figure S2A).[14,37,47,48] Inductively coupled plasma (ICP) measurements (Table S3) show a near-quantitative introduction of Co and Zn. The introduction of Zn and Co centers had a minimal effect on the surface area of the catalysts, which remained within the range of 470−550 $m^2 g^{-1}$ (Table S3 and Table S5).

Consistent with what was observed for Zn-DeAlBEA, IR spectra of the −OH region of DeAlBEA and metal-supported DeAlBEA catalysts (Figures S2B,C) show that the intensity of the band at 3500 cm^{-1}, representing silanol nests, is significantly reduced in intensity after introduction of Zn and/or Co species, indicating the grafting of metal centers onto silanol nests to form M−O−Si interactions at high temperature.[34,37] IR spectra of adsorbed pyridine show bands at 1611 cm^{-1} and 1608 cm^{-1} for pyridine interacting with the Lewis acid centers in Zn-DeAlBEA and Co-DeAlBEA, respectively, together with weak IR bands for pyridine H-bonding with ≡Si−OH groups in the silanol nests (Figure 1B).[37] The changes in IR spectra for Zn-DeAlBEA and Co-DeAlBEA suggest that Zn and Co cations are captured by the silanol nests on the DeAlBEA support during calcination. The IR spectrum of pyridine adsorbed on 0.12Co0.24Zn-DeAlBEA exhibits a combined band at 1610 cm^{-1} for pyridine adsorbed on Zn and Co Lewis acid sites; the integrated area of this peak nearly equals the sum of the integrated peak areas for 0.24Zn-DeAlBEA and 0.12Co-DeAlBEA (Figure 1C), suggesting that Co and Zn in 0.12Co0.24Zn-DeAlBEA are atomically dispersed.

Aberration-corrected high-angle annular dark-field scanning transmission electron microscopy (HAADF-STEM) images of 0.12Co-DeAlBEA and 0.12Co0.24Zn-DeAlBEA are displayed in Figure 1. The low-magnification TEM image (Figure 1D) shows that DeAlBEA is composed of zeolite assemblies of nanocrystals about 20 nm in diameter. The uniform bright dots circled in yellow in Figure 1E suggest that Co is atomically dispersed in 0.12Co-DeAlBEA. For 0.12Co0.24Zn-DeAlBEA, both isolated metal atoms highlighted by yellow circles and proximal atoms highlighted by blue circles were observed (Figure 1F). These results suggest the formation of proximal Zn−(O)−Co dual sites, which is confirmed by XAS characterization discussed below. Furthermore, the HRTEM image shows a uniformly oriented lattice across the zeolite crystal, characteristic of crystalline BEA zeolite (Figure S4). The corresponding TEM-energy-dispersive spectroscopy (EDS) elemental mappings show that Co and Zn atoms are evenly dispersed across the BEA matrix (Figure 1G).

2.2. Structure of Isolated Co Sites and Co−O−Zn Sites. XAS of Co-DeAlBEA and CoZn-DeAlBEA was conducted to identify the chemical state and coordination geometry of the Co and Zn atoms. Figure 2A shows the Co K-edge X-ray absorption near-edge structure (XANES) spectra of 0.12Co-DeAlBEA, 0.12Co0.12Zn-DeAlBEA, and 0.12Co0.24Zn-DeAlBEA. The position of the Co absorption edge for all three samples is close to that of CoO, indicating that the oxidation states of Co sites are close to +2. The enlarged XANES spectrum shows a slight positive shift for CoZn-DeAlBEA relative to Co-DeAlBEA, and the shift increases with increasing Zn loading, suggesting that the oxidation state of Co is altered slightly by its interaction with proximal Zn atoms. This trend is consistent with the observation by XPS that the binding energy of Co $2p_{3/2}$ in 0.12Co0.24Zn-DeAlBEA shifts slightly from 782.1 eV for Co-DeAlBEA to 782.7 eV (Figure S5). Further analysis of XANES data for Co-DeAlBEA and CoZn-DeAlBEA reveals that the valence states of Co species in Co-DeAlBEA and CoZn-DeAlBEA are +1.42 and +1.63 to +1.73, respectively (Figure S6). Figure 2B shows the Co K-edge Fourier transform k^3-weighted EXAFS (FT-EXAFS) spectra of the three samples. The prominent feature at 1.5 Å is a characteristic of backscattering from Co−O neighbors, while the absence of backscattering peaks for Co−O−Co and Co−Co structures suggests that Co^{2+} cations are atomically dispersed. This conclusion is further supported by wavelet-transforms of the Co K-edge EXAFS (WT-EXAFS) spectra of CoZn-DeAlBEA (Figure S7), which correspond to backscattering from the Co and O atoms.

The coordination of Co species was determined by fitting the EXAFS data shown in Figure 2C. The k^3-weighted FT-EXAFS spectra of the Co K-edge for all three catalysts have a distinct peak at 1.5 Å due to a first-shell layer of O atoms.[19] Furthermore, 0.12Co-DeAlBEA shows a weak peak in the second-shell at about 2.5 Å, which is representative of the Co−(O)−Si bond. Table S4 shows that the coordination numbers (CNs) of Co−O and Co−(O)−Si bonds are about 5.1 ± 0.5 and 2.8 ± 1.9 with bond distances of ca. 2.04 ± 0.02 and 3.02 ± 0.03 Å, respectively. The assignment of these peaks is consistent with Co motifs in MFI frameworks and Co@Mo−S-1; the Co−O bond is in the range of 1.78−2.07 Å, while the Co−(O)−Si is 3.08−3.16 Å.[41] Moreover, the UV−vis spectra shown in Figure 2G are consistent with tetrahedrally coordinated Co sites. We note that the XAS analyses of Co-DeAlBEA and CoZn-DeAlBEA were acquired at room temperature after ex situ pretreatment in N_2 at 823 K; hence, it is likely that during the acquisition of EXAFS data, the samples contained adsorbed water. This interpretation is supported by our previous work on Zn-DeAlBEA, in which it was observed that CN_{Zn-O} decreased from 4.2 ± 0.9 to 3.1 ± 0.6 as the temperature for acquisition of the EXAFS data increased from ambient temperature to 773 K, due to the removal of adsorbed water.[37] Accordingly, Co ions in 0.12Co-DeAlBEA are proposed to be present as tetrahedral $(≡SiO)_2$−Co···$(O(H)-Si≡)_2$ species, in which Co also interacts with one water molecule to give a total CN_{Co-O} value of ∼5.

When Co ions are introduced to Zn-DeAlBEA, the CNs and bond distance of Co−O bonds in CoZn-DeAlBEA are similar to those for Co-DeAlBEA, but the center of the second peak shifts to 2.2 Å. Combined with XPS and UV−vis spectroscopy, this peak is possibly due to a combination of Co−(O)−Zn/Si bonds.[42] Further analysis shows that the CNs of Co−(O)−Zn and Co−(O)−Si backscatters are around 1.3 ± 0.2 and 0.7 ± 0.2, respectively, for 0.12Co0.12Zn-DeAlBEA. As the Zn/Al ratio increases to 0.24, the CN of the Co−(O)−Zn bond increases slightly to 1.4 ± 0.5, and that of the Co−(O)−Si decreases to around 0.3 ± 0.1. This observation suggests that Co ions in CoZn-DeAlBEA are mostly bonded to both Zn and Si in a configuration such as ≡SiO−Co−O−Zn−OSi≡,

https://doi.org/10.1021/jacs.5c16367
J. Am. Chem. Soc. 2025, 147, 42110−42122

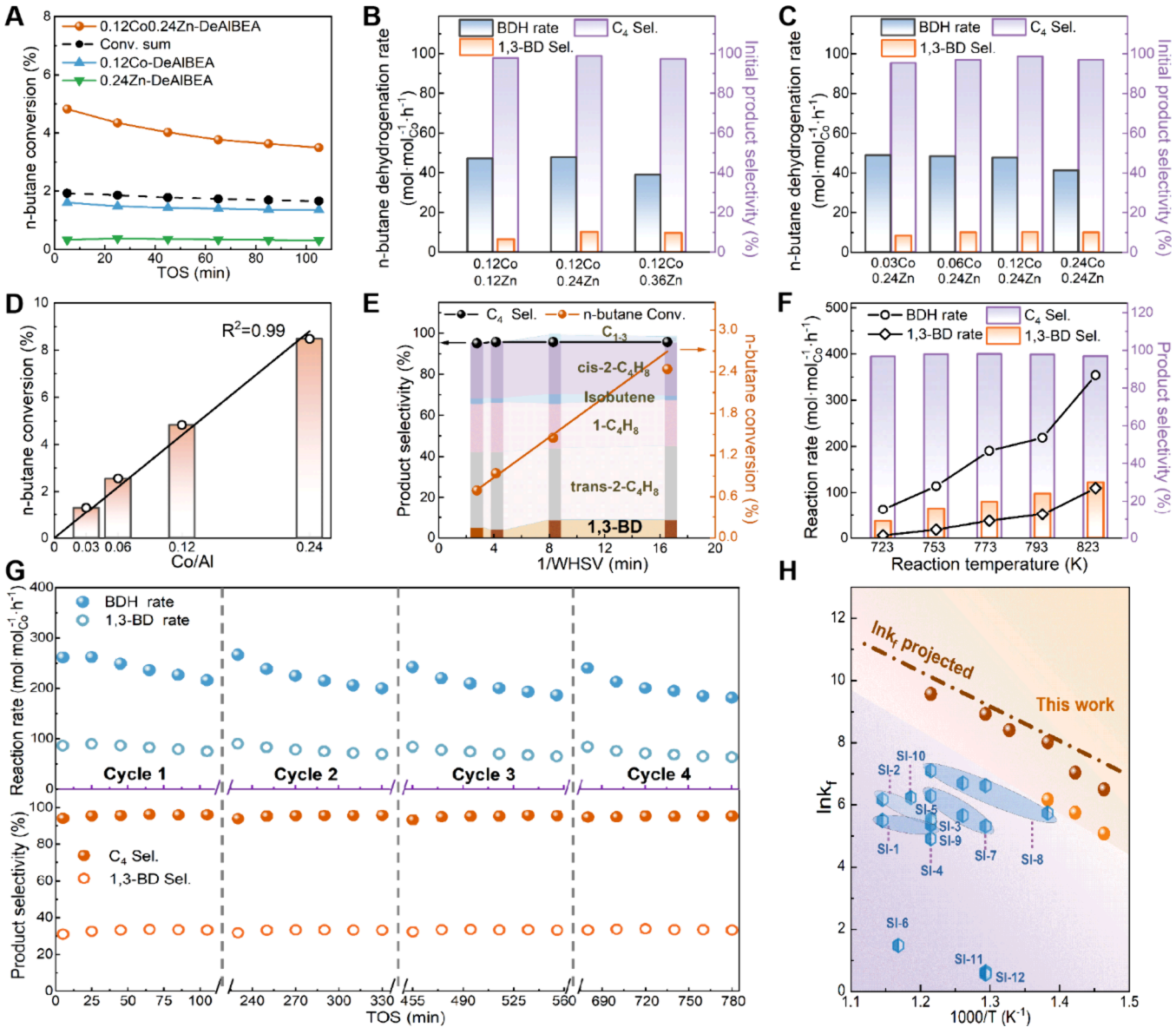

Figure 3. (A) Conversion of *n*-butane over 0.12Co-DeAlBEA, 0.24Zn-DeAlBEA, and 0.12Co0.24Zn-DeAlBEA as a function of time-on-stream (TOS), measured at 723 K with 2.5 kPa of *n*-butane/N_2. Effect of (B) Zn and (C) Co loading on the initial rate of *n*-butane dehydrogenation and dehydrogenation selectivity. (D) Effect of Co loading on the *n*-butane conversion over *x*Co0.24Zn-DeAlBEA. Effect of (E) spacetime and (F) reaction temperature on *n*-butane dehydrogenation conversion and product selectivity over 0.03Co0.24Zn-DeAlBEA, measured with 2.5 kPa *n*-butane/N_2. (G) The regenerability of 0.03Co0.24Zn-DeAlBEA for *n*-butane dehydrogenation was measured at 823 K with 2.5 kPa *n*-butane/N_2. (H) Comparison of the forward rate coefficient for *n*-butane dehydrogenation with other reported non-noble-metal-based catalysts. Dark red balls, orange balls, and blue hexagons represent CoZn-DeAlBEA, Co-DeAlBEA, and previously reported non-noble-metal catalysts, respectively.

formed upon condensation of Co cations with the ≡SiOZn−OH group and silanol group.

Further evidence for the generation of the Co−(O)−Zn linkage was obtained from Zn K-edge XAS of 0.12Co0.24Zn-DeAlBEA. As shown in Figure 2D, the position of the Zn absorption edge for this material coincides with that for ZnO, indicating that Zn is present predominantly as Zn^{2+}.[43] The FT-EXAFS spectrum exhibits a dominant Zn−O first-shell peak in the range of 1.0−2.0 Å but no Zn−Zn or Zn−O−Zn backscattering peaks (Figure 2E). The WT-EXAFS of the Zn K-edge shown in Figure S8 further confirms the presence of Zn−O bonds. In addition to the Zn−O bond in the first shell of 0.12Co0.24Zn-DeAlBEA, the real and fitted k^3-weighted Fourier transform spectrum shown in Figure 2F evidences a contribution due to Zn−(O)−M backscattering. The CN for Zn−(O)−M bonds in 0.12Co0.24Zn-DeAlBEA is about 3.9 ± 0.5 (Table S4). The fitted Zn−(O)−M bonds with a general bond distance of 2.94 ± 0.02 Å are identified to be an average of Zn−(O)−Si (3.12 ± 0.11 Å) and Zn−(O)−Co (2.73 ± 0.03 Å) bonds based upon the XAS analysis of Zn-DeAlBEA[37] and the analysis of the Co K-edge for CoZn-DeAlBEA reported above. A comparison of the Zn K-edge EXAFS spectra for 0.36Zn-DeAlBEA with those for 0.12Co0.24Zn-DeAlBEA is given in Figure S9. This confirms that Zn maintains a stable interaction with the backbone Si, as well as Zn−(O)−Co interaction in the bimetallic catalyst.

UV−vis spectra of DeAlBEA and Zn/Co-DeAlBEA were employed to characterize the coordination environment of the

https://doi.org/10.1021/jacs.5c16367
J. Am. Chem. Soc. 2025, 147, 42110−42122

Co and Zn species. As shown in Figure 2G, the UV−vis spectrum of 0.12Co-DeAlBEA shows three bands at 653, 592, and 518 nm, a typical triplet representing the unique d−d transition of tetrahedral Co^{2+}, supporting the proposal that Co ions are tetrahedrally coordinated on the framework of DeAlBEA via Co−O−Si bonds.[44−46] The broad peaks at both 310 and 365 nm may be related to the charge transfer between O and Co ions.[46,47] The UV−vis spectrum of 0.24Zn-DeAlBEA demonstrates that Zn is dispersed in the form of isolated atoms, as indicated by the absorption band below 210 nm that is characteristic of charge transfer from O^{2-} in the zeolite framework to Zn^{2+}.[16,48] In sharp contrast to monometallic Co-DeAlBEA, the set of three bands no longer appears for CoZn-DeAlBEA, while the signals at ca. 310 and 365 nm are more intense. These observations suggest that grafting Co into ≡SiOZn−OH nests creates new Co−O−Zn bonds. Taking the XAS and UV−vis spectroscopy experiments into consideration, Co in CoZn-DeAlBEA is proposed to be grafted to the zeolite framework and to Zn, i.e., (≡SiO)−CoOZn−(SiO≡), with Co also possibly datively bonded with one silanol group and up to two water molecules.

To summarize, the characterization data presented above suggest that Co ions react with ≡Si−OH and ≡Si−OH/≡SiOZn−OH groups to form isolated Co cations in Co-DeAlBEA and CoZn-DeAlBEA, respectively, as illustrated in Figure 2H. For Co-DeAlBEA, isolated Co ions react with ≡Si−OH groups in the silanol nests of DeAlBEA via two Co−O−Si bonds and interact datively with two residual ≡Si−OH groups, i.e., $(\equiv SiO)_2-Co\cdots(O(H)-Si\equiv)_2$. When Zn sites are introduced into the silanol nests of DeAlBEA and utilized as support, the ≡SiOZn−OH groups and proximal ≡Si−OH groups could stabilize Co sites to form (≡SiO)−CoOZn−(SiO≡) structures.

2.3. *n*-Butane Dehydrogenation to 1,3-BD. *n*-Butane dehydrogenation was investigated on 0.12Co-DeAlBEA, 0.24Zn-DeAlBEA, and 0.12Co0.24Zn-DeAlBEA using identical reaction conditions chosen so that the *n*-butane conversion was always differential (<5%). For all catalysts, the main products are *trans*-2-butene, 1-butene, *cis*-2-butene, 1,3-BD, and a small amount of isobutene. The overall selectivity to these products is >90%. 0.12Co0.24Zn-DeAlBEA exhibits an initial *n*-butane conversion of 4.8%, which is much higher than the sum of *n*-butane conversions over 0.12Co-DeAlBEA and 0.24Zn-DeAlBEA (1.9%, Figure 3A), suggesting that Co−O−Zn sites in 0.12Co0.24Zn-DeAlBEA are more active compared to the corresponding monometallic sites. Furthermore, 0.12Co0.24Zn-DeAlBEA exhibits a higher dehydrogenation selectivity relative to that of 0.12Co-DeAlBEA and 0.24Zn-DeAlBEA (98.8% vs 97.9% and 90.6%, Figure S10). When normalized by the moles of metal, the turnover frequency (TOF) for *n*-butane dehydrogenation over 0.12Co0.24Zn-DeAlBEA (47.8 $mol\cdot mol_{Co}^{-1}\cdot h^{-1}$) is about 3 and 34 times higher than that over 0.12Co-DeAlBEA and 0.24Zn-DeAlBEA, respectively (Figure S10).

To explore whether mobilization of initially deposited Zn species occurred during the subsequent introduction of Co species into Zn-DeAlBEA, 0.12Co0.24Zn-DeAlBEA was prepared via co-impregnating DeAlBEA with an aqueous solution containing both Co and Zn precursors, followed by drying and calcination under conditions identical to those used for the preparation of 0.12Co0.24Zn-DeAlBEA by sequential impregnation of DeAlBEA with Zn and then Co. As illustrated in Figure S11, both preparations of 0.12Co0.24Zn-DeAlBEA show nearly identical *n*-butane conversion, overall selectivity to C_4 dehydrogenation products, and selectivity of 1,3-BD. These findings suggest that independent of whether Co^{2+} cations are impregnated into Zn-DeAlBEA or are co-impregnated with Zn^{2+} cations, the final structural environments of Zn and Co in CoZn-DeAlBEA are the same.

To explore whether the Co or Zn atom of the bimetallic species is the intrinsic active center, *n*-butane dehydrogenation over *x*Co*y*Zn-DeAlBEA with different Co or Zn loadings was investigated. As seen in Figure 3B, 0.12Co*y*Zn-DeAlBEA (y = 0.12−0.36) with Co/Al = 0.12 exhibit a mild decrease in *n*-butane dehydrogenation activity with an increasing Zn/Al ratio (TOF = 47.8−39.0 $mol\cdot mol_{Co}^{-1}\cdot h^{-1}$). On the other hand, the conversion of *n*-butane over *x*Co0.24Zn-DeAlBEA increases in proportion to the Co/Al ratio (Figure 3D), and Figure 3C shows that the TOF for *n*-butane dehydrogenation per Co ion is nearly the same for Co/Al = 0.03 to 0.12, 49.0 $mol\cdot mol_{Co}^{-1}\cdot h^{-1}$ to 47.8 $mol\cdot mol_{Co}^{-1}\cdot h^{-1}$, but decreases slightly to 41.4 $mol\cdot mol_{Co}^{-1}\cdot h^{-1}$ when the Co/Al ratio is increased to 0.24. These results demonstrate that Co ions in the (≡SiO)−CoOZn−(SiO≡) sites over CoZn-DeAlBEA are the active centers.

2.4. Effects of Spacetime and Temperature on *n*-Butane Dehydrogenation. The effects of spacetime (expressed as the inverse of the WHSV) on *n*-butane conversion over CoZn-DeAlBEA at 723 K are shown in Figure 3E. The conversion of *n*-butane increases linearly within the spacetime up to $(WHSV)^{-1}$ 17 min. Independent of spacetime, the selectivity to C_4 products decreases in the order of *trans*-2-butene > *cis*-2-butene > 1-butene > 1,3-BD > isobutene. As the spacetime increases, the selectivity of 1,3-BD increases from 4.2% to 8.9%, whereas the selectivity to linear butenes decreases. These observations suggest that *trans*-2-butene, *cis*-2-butene, and 1-butene are the primary products, whereas 1,3-BD forms via secondary dehydrogenation of linear butenes, in agreement with what has been observed for Zn-DeAlBEA.[37] For spacetimes > 8 min, the selectivity to C_4 butenes and 1,3-BD both reach a plateau of 87.4% and 8.4%, respectively, close to the thermodynamic equilibrium distribution for these products at 723 K (91.3% and 8.7%).[34]

The effects of reaction temperature on BDH performance were examined for 0.03Co0.24Zn-DeAlBEA using a WHSV of 2.8 h^{-1} and 2.5 kPa of *n*-butane. As shown in Figure 3F, the net rate of *n*-butane dehydrogenation increases with increasing reaction temperature, reaching a value of 354 $mol\cdot mol_{Co}^{-1}\cdot h^{-1}$ at 823 K. Notably, high reaction temperature is favorable for the selective formation of 1,3-BD. The rate of 1,3-BD formation increases significantly from 5.9 to 110.0 $mol\cdot mol_{Co}^{-1}\cdot h^{-1}$ as the temperature increases from 723 to 823 K, the selectivity to 1,3-BD rising to ∼31% at 823 K, which is superior to that for isolated ≡SiOZn−OH sites (ca. 12%).[37] This high 1,3-BD selectivity is comparable to that observed for isolated Pt sites grafted onto Zn nests (ca. 35.5%) tested under similar reaction conditions.[34] Over the temperature range investigated, the ratios of 2-butene/1-butene and *trans*-2-butene/*cis*-2-butene remain close to the thermodynamic equilibrium distribution (Figure S12).

Based on the effects of reaction temperature and spacetime, the stability and regenerability of CoZn-DeAlBEA for BDH were investigated via four sequential BDH reaction−oxidative regeneration experiments carried out at 823 K and a WHSV of 1.4 h^{-1} (Figure 3G). As shown, the catalyst exhibits a high initial activity of 261 $mol\cdot mol_{Co}^{-1}\cdot h^{-1}$ and 89 $mol\cdot mol_{Co}^{-1}\cdot h^{-1}$ for *n*-butane dehydrogenation and 1,3-BD formation, as well as

https://doi.org/10.1021/jacs.5c16367
J. Am. Chem. Soc. 2025, 147, 42110−42122

Table 1. Experimentally Measured and Theoretically Predicted Activation Energies and Adsorption Enthalpies for *n*-Butane and 1-Butene Dehydrogenation over 0.03Co-DeAlBEA and 0.03Co0.12Zn-DeAlBEA and Experimentally Measured Activation Energies and Adsorption Enthalpies over 0.12Zn-DeAlBEA

		E_{app} [a] (kJ·mol^{-1})		ΔH_{ads}* [b] (kJ·mol^{-1})		E_{int} [c] (kJ·mol^{-1})	
catalyst	reaction	experiment	theory	experiment	theory	experiment	theory
Co-DeAlBEA	*n*-Butane DH	111	114.2	—	−50.4	—	164.6
CoZn-DeAlBEA		91	68.9	−43	−59.9	134	128.8
Zn-DeAlBEA[d]		132	—	—	—	—	—
Co-DeAlBEA	1-Butene DH	51	73.8	−63	−55.2	114	129.0
CoZn-DeAlBEA		18	19.5	−64	−57.3	82	76.8
Zn-DeAlBEA[d]		72	—	−72	—	144	—

[a] E_{app} is the apparent activation energy. [b] ΔH^*_{ads} is the adsorption enthalpy of *n*-butane or 1-butene obtained from fits of adsorption equilibrium constants ($K_{C_4^-}$ and $K_{C_4^=}$). [c] E_{int} is the intrinsic activation energy obtained from zero-order rate constant ($k_{C_4^-}$ and $k_{C_4^=}$). [d] Kinetics data of 0.12Zn-DeAlBEA from Zhang et al. reported in ref 37.

a high and stable selectivity to 1,3-BD of 33.3%.[37] After each test of the *n*-butane dehydrogenation reaction, the catalyst was regenerated in flowing air (30 mL·min^{-1}) at 823 K for 1 h. No significant deactivation was observed after three regeneration cycles, indicating that CoZn-DeAlBEA can be regenerated without a loss of activity or selectivity. The regenerability of CoZn-DeAlBEA was also investigated following its operation at high *n*-butane conversion. As shown in Figure S13A, 0.03Co0.24Zn-DeAlBEA exhibits an initial conversion of *n*-butane of 62.6% and overall selectivity to C_4 dehydrogenation products of 91.1%. In comparison to the BDH conducted at low conversion (see Figure 3G), the selectivity of 1,3-BD decreases from 33.3% to 21.9−28.9% due to the reversible hydrogenation of 1,3-BD to butenes. Figure S13A shows that the activity and selectivity of the catalyst could be recovered after each of the four dehydrogenation cycles conducted with a high conversion of *n*-butane.

The long-term stability of CoZn-DeAlBEA was also investigated at 823 K. As shown in Figure S13B, 0.03Co0.24Zn-DeAlBEA exhibits an initial *n*-butane conversion of around 35.4%, which decreases to 20.4% after 200 min and gradually to 10.8% when the TOS is extended to 1200 min. Elemental analysis confirms the absence of metal loss during the prolonged reaction period. Thermogravimetry analysis (TGA) of spent catalyst shown in Figure S14 reveals that the coke deposition is about 3.67 wt % after 1200 min and contributes mainly to the gradual deactivation of catalyst with extended TOS. Calcining the spent catalyst restored its full initial activity. An additional test of the stability of this catalyst was conducted using pure *n*-butane (101.3 kPa). As seen in Figure S15, here too, the catalyst could be used over four reaction−regeneration cycles with minimal loss of activity.

The activity of CoZn-DeAlBEA and Co-DeAlBEA for BDH was also compared with those of previously reported non-noble-metal-based catalysts. The elemental composition of each catalyst and their reaction conditions were summarized in Table S5. Because alkane dehydrogenation is highly reversible and the reaction conditions used by different authors differ significantly, the effective forward rate coefficient, k_f, for *n*-butane dehydrogenation was calculated for each catalyst. The derivation of k_f is based on a plug flow reactor model.[34] Figure 3H and Figure S16A show the forward rate coefficients for *n*-butane dehydrogenation of different catalysts operated under a range of temperature. The dashed line represents the projected values of k_f based on the experimentally estimated apparent activation energy of *n*-butane dehydrogenation for 0.03Co0.12Zn-DeAlBEA (Table 1). The data show that 0.03Co0.12Zn-DeAlBEA exhibits the highest activity for *n*-butane dehydrogenation of all catalysts considered. As analyzed, the forward rate coefficient for *n*-butane dehydrogenation over 0.03Co0.12Zn-DeAlBEA at 823 K is around 1.4 × 10^4 mol·mol$_{Co}^{-1}$·h^{-1}·bar^{-1}, which is higher than that for the previously reported non-noble-metal-based catalysts by 1 to 2 orders of magnitude. Moreover, Figure S16B compares the ln k_f for BDH over CoZn-DeAlBEA and Pt-based catalysts reported in the literature. Notably, CoZn-DeAlBEA exhibits comparable activity with most Pt-based catalysts.

2.5. Kinetics and Mechanism of *n*-Butane Dehydrogenation over Co-DeAlBEA and CoZn-DeAlBEA. The spacetime study presented here and in our previous reports[34,37] show that 1,3-BD is produced by a two-step process: *n*-butane first undergoes dehydrogenation primarily to 1-butene, which then rapidly isomerizes to produce an equilibrated mixture of 1-butene and 2-butene isomers; subsequently, 1-butene undergoes secondary dehydrogenation to produce 1,3-BD. To better understand the superior catalytic dehydrogenation activity of Co−O−Zn sites, the kinetics of *n*-butane dehydrogenation to butene and 1-butene dehydrogenation to 1,3-BD were investigated over monometallic Co-DeAlBEA and bimetallic CoZn-DeAlBEA.

The kinetics of *n*-butane dehydrogenation to butenes over 0.03Co0.12Zn-DeAlBEA was investigated under differential reaction conditions (Figure 4A). At all three temperatures (683, 703, and 723 K), the rate of *n*-butane dehydrogenation exhibits a Langmuir dependence on the *n*-butane partial pressure. At the lowest temperature of 683 K, a plateau is approached for *n*-butane partial pressures higher than 9 kPa. Independent of *n*-butane partial pressure, the observed molar ratios of 2-butene/1-butene are close to their equilibrium value, verifying the rapid isomerization of linear butenes (Figure S17). Concurrently, the molar ratios of 2-butene/1-butene exhibit a dependence on temperature, decreasing from 3.0 to 2.7 as temperature increases from 683 to 723 K. The Mears criterion was used to test for external mass transfer limitation, but as noted in the Supporting Information, under the reaction conditions used, no external mass transfer limitation was observed.

The results for *n*-butane dehydrogenation over CoZn-DeAlBEA shown in Figure S17 and our previous findings for Zn-DeAlBEA[37] show that isomerization of 1-butene to thermodynamically more stable 2-butene occurs over acid sites and reaches thermodynamic equilibrium. This phenomenon also occurs during 1-butene dehydrogenation over Co-based catalysts. To determine the kinetics of 1-butene

https://doi.org/10.1021/jacs.5c16367
J. Am. Chem. Soc. 2025, 147, 42110−42122

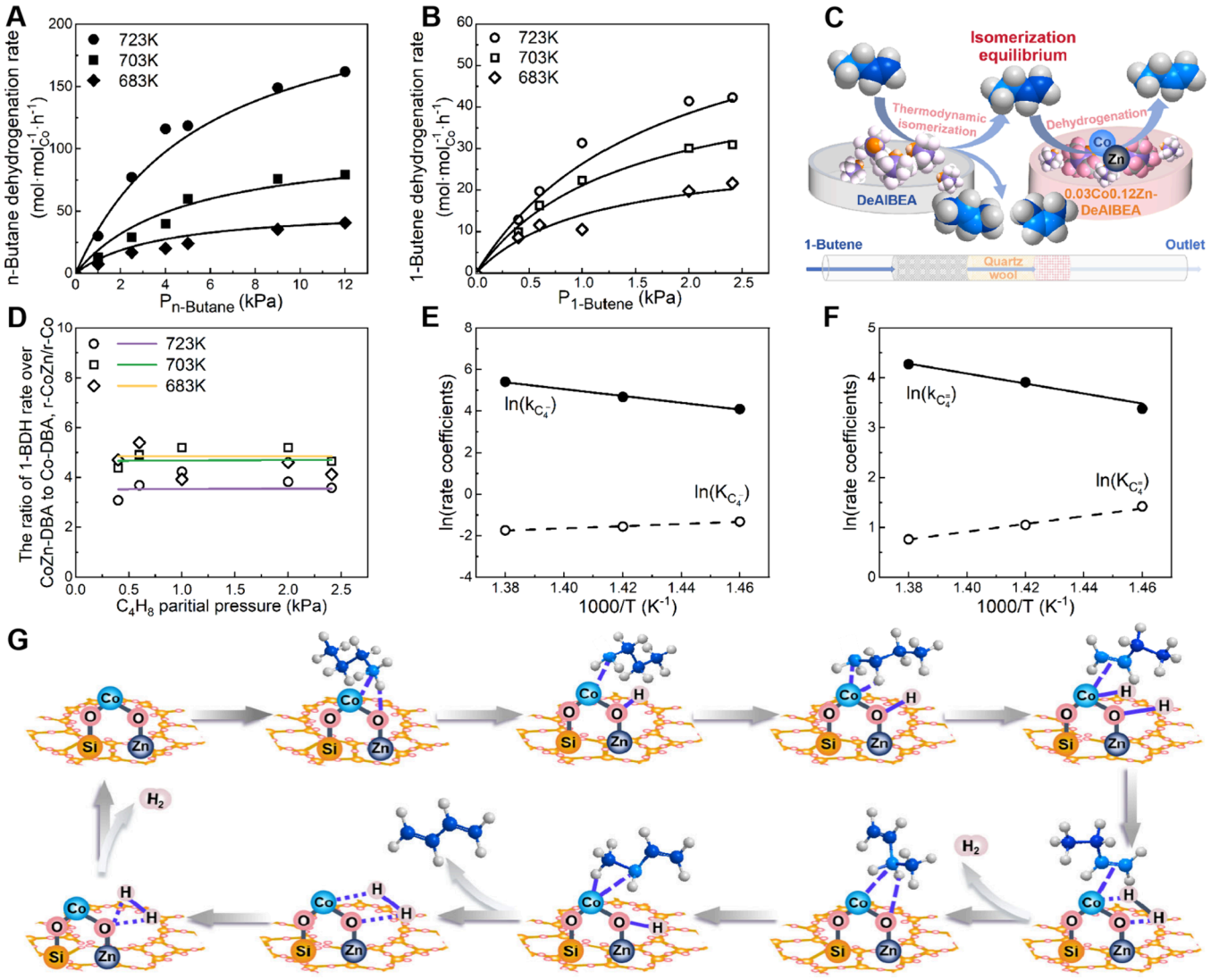

Figure 4. (A) Dependence of the rate of *n*-butane dehydrogenation on *n*-butane partial pressure, at 683, 703, and 723 K over 0.03Co0.12Zn-DeAlBEA. Solid lines are regressed fits of eq 1 to the data. (B) Dependence of the rate of 1-butene dehydrogenation on the 1-butene partial pressure, measured at 683, 703, and 723 K over 0.03Co0.12Zn-DeAlBEA. Solid lines are regressed fits of eq 2 to the data. (C) Schematic illustration of the catalyst bed for the studies of the kinetics of 1-butene dehydrogenation. (D) Dependence of the rate of 1-butene dehydrogenation over CoZn-DeAlBEA to that over Co-DeAlBEA (r-CoZn/r-Co) as functions of 1-butene partial pressure and temperature. (E) An Arrhenius plot of the rate coefficient ($k_{C_4^-}$) for *n*-butane dehydrogenation vs $1/T$ and a van't Hoff plot of the *n*-butane adsorption constant ($k_{C_4^-}$) vs $1/T$ for 0.03Co0.12Zn-DeAlBEA. (F) An Arrhenius plot of the rate coefficient ($k_{C_4^=}$) for 1-butene dehydrogenation vs $1/T$ and a van't Hoff plot of the 1-butene adsorption constant ($k_{C_4^=}$) vs $1/T$ for 0.03Co0.12Zn-DeAlBEA. (G) The proposed reaction mechanism for *n*-butane dehydrogenation over Co−O−Zn sites.

dehydrogenation to 1,3-BD, a dual-layer catalyst bed containing 100 mg of DeAlBEA was placed above a layer of 10 mg of 0.03Co0.12Zn-DeAlBEA, separated by an inert quartz wool (Figure 4C). The DeAlBEA bed served to isomerize butene isomers to their equilibrium distribution; further 1-butene isomerization did not occur over the Co-based catalyst because the residence time in that bed was low due to its small mass and, therefore, it operated in the regime of differential conversion. The upper-layer DeAlBEA serves to catalyze 1-butene isomerization to an equilibrated mixture of 1- and 2-butene, whereas 0.03Co0.12Zn-DeAlBEA catalyzes the 1-butene dehydrogenation to 1,3-BD.[34,35,37] Figure S18 shows the effects of spacetime on 1-butene conversion over a dual-layer catalyst bed. The reversible hydrogenation and deep dehydrogenation processes are insignificant for $(WHSV)^{-1}$ < 12 min, and the molar ratios of 2-/1-butene obtained experimentally are close to their thermodynamic equilibrium values. Based upon the spacetime investigation, the kinetics of 1-butene dehydrogenation were measured at 683−723 K. Figure 4B shows that the rate of 1-butene dehydrogenation increases linearly with 1-butene partial pressure at low 1-butene partial pressures, after which it increases further with less than a first-order dependence at all three temperatures. To further verify the establishment of equilibrium isomerization, the molar ratios of 2-butene/1-butene at each temperature and 1-butene partial pressure are calculated. As shown in Figure S18C, the 2-/1-butene molar ratio is almost independent of 1-butene partial pressure and close to the equilibrium value.

The kinetics of *n*-butane dehydrogenation over isolated $(\equiv SiO)_2$−Co···$(O(H)-Si\equiv)_2$ sites are shown in Figure S19A. In

https://doi.org/10.1021/jacs.5c16367
J. Am. Chem. Soc. 2025, 147, 42110−42122

sharp contrast to what is observed over bimetallic CoZn-DeAlBEA, the rates of *n*-butane dehydrogenation increase linearly with *n*-butane partial pressure up to 12 kPa for the three temperatures, 683, 703, and 723 K, investigated, parallel to what was observed for isolated ≡SiOZn−OH sites.[34] The obvious difference in *n*-butane dehydrogenation kinetics over Co-DeAlEBA and CoZn-DeAlBEA illustrates that the structural features of Co−O−Zn sites contribute to a much stronger interaction between *n*-butane and the catalyst. The promotion of alkane adsorption, including propane and *n*-butane, has been observed upon the generation of ≡SiOZn−OH nests from isolated Zn sites.[34] Based on the rate law (eq 3) for BDH over Co-DeAlBEA and the rate coefficients (k_{BDH}), the apparent activation energy for *n*-butane dehydrogenation over Co-DeAlBEA is estimated to be about 111 kJ·mol^{-1} (Figure S19B).

A similar dual-layer catalyst bed comprising DeAlBEA and 0.03Co-DeAlBEA was used to determine the kinetics of 1-butene dehydrogenation over isolated Co sites. As shown in Figure S20A, 1-butene dehydrogenation over 0.03Co-DeAlBEA also exhibits a Langmuir dependence on the 1-butene partial pressure. Analysis of the kinetics of 1-butene dehydrogenation over Co-DeAlBEA and CoZn-DeAlBEA shows no significant difference in the adsorption of 1-butene over isolated Co sites and Co−O−Zn sites. This may be due to the strong adsorption of olefins on Lewis acid sites, which excludes the minor difference in the electronic states of isolated Co sites and bimetallic Co−O−Zn sites.

The performances of *n*-butane dehydrogenation for Co-DeAlBEA and CoZn-DeAlBEA are compared in Figure 3A. It is seen that the Co−O−Zn structure enhances the rate of *n*-butane dehydrogenation to butenes compared to that for isolated Co ions; however, the effect of different Co structures on the activity for 1-butene dehydrogenation to 1,3-BD remains unclear. Figure 4D shows the dependence of the ratio of the 1-butene dehydrogenation rate over CoZn-DeAlBEA to that over Co-DeAlBEA (r-CoZn/r-Co), as functions of the 1-butene partial pressure and temperature. It is noted that the r-CoZn/r-Co ratio is always larger than 1 (3.6−4.7), confirming that Co−O−Zn sites are more active for 1-butene dehydrogenation compared to isolated Co sites. We also note that identical 1-butene dehydrogenation activities are observed for isolated and nested ≡SiOZn−OH sites.[34] This finding demonstrates that the interaction between Co and Zn atoms in Co−O−Zn sites promotes both *n*-butane dehydrogenation to butenes and 1-butene dehydrogenation to 1,3-BD reactions. In addition, the r-CoZn/r-Co ratio is nearly independent of the 1-butene partial pressure, but this ratio decreases with increasing temperature from ∼4.7 at 683 K to ∼3.6 at 723 K, which indicates a lower apparent activation energy for 1-butene dehydrogenation over CoZn-ZnDeAlBEA than over Co-DeAlBEA.

Figure 4G illustrates a proposed mechanism for BDH to form 1,3-BD. The reaction begins with the physical adsorption of *n*-butane onto the bimetallic Co−O−Zn sites. Subsequently, the C atom of a methyl group interacts with Lewis acidic Co and a H atom of a methyl group interacts with the O atom connecting Co and Zn atoms. Following this step, the cleavage of a methyl C−H bond of the adsorbed *n*-butane generates C_4H_9* and Co−O(H*)−Zn intermediates, which is assumed to be the possible rate-limiting step.[49−51] Next, abstraction of a H atom from the adjacent methylene group of the C_4H_9* intermediate occurs, producing adsorbed 1-butene and 2H*. In the subsequent step, 1-butene desorbs, followed by the recombination of two H* to form adsorbed H_2 that then desorbs. Adsorbed 1-butene can also undergo further heterolytic C−H cleavage at the methylene group and b-hydride abstraction to produce 1,3-BD and H_2.[34,49] Similarly, the first C−H bond cleavage at the methylene group of 1-butene is regarded as the rate-limiting step in the second dehydrogenation reaction. Finally, desorption of the second H_2 molecule closes the cycle, reforming the ≡SiO−Co−O−Zn−OSi≡ sites. In contrast to what occurs on Co−O−Zn sites, the rate-limiting cleavage of the first C−H bond over isolated Co sites occurs on the atom containing the *n*-butane between Co and Si atoms, which leads to higher activation energies for both *n*-butane dehydrogenation and 1-butene dehydrogenation.

The mechanism shown in Figure 4G was used to derive rate expressions for *n*-butane dehydrogenation and 1-butene dehydrogenation reactions, eqs 1 and 2, respectively. Over isolated Co sites, the second term in the denominator of eq 1 should be insignificant due to the weak adsorption of *n*-butane on such sites (Figure S19A). Accordingly, eq 1 then simplifies to eq 3 to describe the kinetics of *n*-butane dehydrogenation over Co-DeAlBEA.

$$r_{C_4^-} = \frac{k_{C_4^-} K_{C_4^-} P_{C_4^-}}{1 + K_{C_4^-} P_{C_4^-}} \tag{1}$$

$$r_{C_4^=} = \frac{k_{C_4^=} A K_{C_4^=} P_{C_4^=}}{1 + K_{C_4^=} P_{C_4^=}} \tag{2}$$

$$r_{C_4^-} = k_{C_4^-} K_{C_4^-} P_{C_4^-} \tag{3}$$

The parameters $k_{C_4^-}$ and $k_{C_4^=}$ represent the rate coefficients associated with the first C−H bond cleavage during *n*-butane dehydrogenation and 1-butene dehydrogenation, respectively, for which $k_{C_4^-}$ and $k_{C_4^=}$ are the equilibrium constants for *n*-butane and 1-butene physisorption onto active sites, respectively. *A* is the molar ratio of the 1-butene partial pressure achieved thermodynamic equilibration of linear butenes relative to the initial 1-butene partial pressure fed into the reactor at a specific temperature. $P_{C_4^-}$ and $P_{C_4^=}$ represent the partial pressures of *n*-butane and 1-butene fed, respectively. Inspection of eqs 1 and 2 shows that a first-order dependence of the rate of dehydrogenation on reactant partial pressure and inhibition of these rates at high reactant partial pressures due to occupancy of active sites by reactant-derived species is predicted. In the case of Co-DeAlBEA, the relatively weak binding of *n*-butane to isolated Co sites leads to a first-order dependence of the rate of *n*-butane dehydrogenation on the *n*-butane concentration.

The kinetic data were fit to eqs 2 and 3. Tables S6−S9 summarize the fitted rate coefficients and adsorption equilibrium constants for the dehydrogenation of *n*-butane and 1-butene over both 0.03Co-DeAlBEA and 0.03Co0.12Zn-DeAlBEA catalysts. The estimated parameters provide good descriptions of the rates of *n*-butane and 1-butene dehydrogenation, as demonstrated by the parity plots shown in Figure S21.

Experimentally measured activation energies (E_{app}, E_{int}) and adsorption enthalpies (ΔH^*_{ads}) for *n*-butane and 1-butene dehydrogenation were estimated from Arrhenius and van't Hoff plots, respectively (Figures 4E,F, Figures S19B, 20C, and 20D) and are listed in Table 1. For *n*-butane dehydrogenation

https://doi.org/10.1021/jacs.5c16367
J. Am. Chem. Soc. 2025, 147, 42110−42122

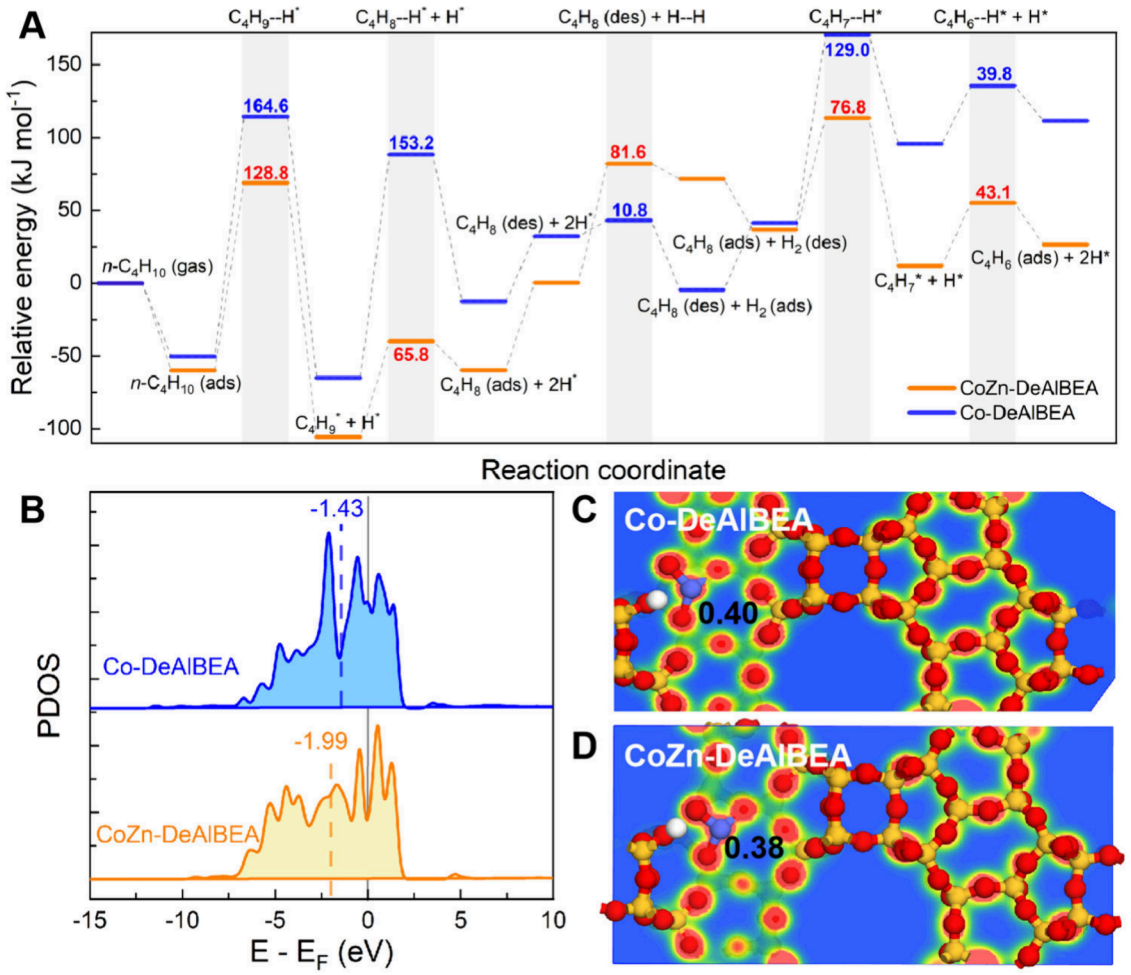

Figure 5. (A) Free-energy profiles for dehydrogenation of *n*-butane or n-butene on CoZn-DeAlBEA and Co-DeAlBEA. (B) PDOS analysis of the Co site on Co-DeAlBEA and CoZn-DeAlBEA. Differential charge density maps and Mulliken charge of (C) Co-DeAlBEA and (D) CoZn-DeAlBEA.

over Co−O−Zn sites, the experimentally measured intrinsic activation energy is 134 kJ·mol^{-1}, whereas the adsorption enthalpy of *n*-butane is −43 kJ·mol^{-1}. Apparent activation energy for *n*-butane dehydrogenation is 91 kJ·mol^{-1}. Previous studies have shown that the adsorption enthalpy of *n*-butane on metal oxides ranges from −34 to −51 kJ·mol^{-1} and that adsorption enthalpy for *n*-butane on Co is comparable to that on ZnO.[52] It is noteworthy that the apparent activation energy for *n*-butane dehydrogenation over isolated $(\equiv SiO)_2$−Co···$(O(H)-Si\equiv)_2$ sites (111 kJ·mol^{-1}) is much higher than that on Co−O−Zn sites (91 kJ·mol^{-1}), consistent with its lower dehydrogenation activity.

In the case of 1-butene dehydrogenation, the adsorption enthalpy for 1-butene over Co−O−Zn sites is −64 kJ·mol^{-1}, which is nearly identical to that for isolated $(\equiv SiO)_2$−Co···$(O(H)-Si\equiv)_2$ sites (−63 kJ·mol^{-1}). This similarity is attributed to the strong interaction of the C=C bond in 1-butene with Lewis acid sites. The adsorption of 1-butene on isolated ≡SiOZn−OH sites is about −72 kJ·mol^{-1}, which is more negative than reported for metal oxide of −50 to −60 kJ·mol^{-1}.[25,53] We note that the intrinsic activation energy for 1-butene dehydrogenation over Co−O−Zn sites (82 kJ·mol^{-1}) is significantly lower than that reported for Cr-based catalysts (134 kJ·mol^{-1}) and monometallic Co-/Zn-DeAlBEA (114 and 144 kJ·mol^{-1}) and comparable to that for single-site PtZn-DeAlBEA (90.3 kJ·mol^{-1}).[34,51]

Periodic density functional theory (DFT) calculations were performed (Figure 5) to compare the experimentally derived activation energies and adsorption enthalpies to their values predicted theoretically. Theoretical values of the activation and adsorption enthalpies of *n*-butane and 1-butene dehydrogenation are given in Table 1. Consistent with the assumption of the mechanism used to interpret the rate data, cleavage of the first C−H bond is the rate-limiting step for both *n*-butane and 1-butene dehydrogenation. We note that the adsorption of *n*-butane on CoZn-DeAlBEA is much stronger than that on Co-DeAlBEA. This difference is attributed to the higher oxidation state of Co on CoZn-DeAlBEA, which is consistent with the XPS and XANES measurements (see Figures S5 and S6). Figures 5B−D show the projected density of states (PDOS) for the d-orbitals of Co in Co-DeAlBEA and CoZn-DeAlBEA. We note that the d-orbital of Co is farther from the Fermi level and the Mulliken charge of Co is lower for CoZn-DeAlBEA than for Co-DeAlBEA, which means the Co in CoZn-DeAlBEA is the good electron acceptor. Table 1 also shows that the DFT-predicted activation energy and adsorption enthalpies are close to the experimentally derived values.

The above results are consistent with the idea that the dehydrogenation activity per Co ion for both *n*-butane and 1-

https://doi.org/10.1021/jacs.5c16367
J. Am. Chem. Soc. 2025, 147, 42110−42122

butene increases by a factor of around 3−4 times for Co−O−Zn sites relative to isolated Co sites. Insights into the catalytic performance of Co-DeAlBEA and CoZn-DeAlBEA were developed from analyses of the reaction kinetics. The strength of *n*-butane adsorption and the activation energy for cleavage of the first C−H bond are both promoted by the interaction of Co with Zn in Co−O−Zn sites present in CoZn-DeAlBEA. By contrast, the enthalpies of 1-butene adsorption on Co−O−Zn sites and Co isolated sites are similar, which is attributed to the strong interaction of the double bond of 1-butene with the Lewis acidic Co site. Nevertheless, Co−O−Zn sites exhibit an activation barrier for cleavage of a C−H bond in the methyl group of 1-butene that is lower than that observed for isolated Co sites.

3. CONCLUSIONS

In this study, we have developed bimetallic Co−O−Zn sites bonded to DeAlBEA that are highly active and selective for *n*-butane dehydrogenation to 1,3-BD. These sites were created by incorporating Co into nested ≡SiOZn−OH sites generated by grafting Zn into the silanol nests of DeAlBEA. The structure of such active sites was determined to be ≡SiO−Co−O−Zn−OSi≡ based on characterization by IR, XAS, UV−vis, and XPS spectroscopy. The resulting interaction between Co and Zn enables the Co ions to adsorb *n*-butane more strongly but adsorb butenes with comparable strength. The interaction of Co with Zn also lowers the activation barrier for cleavage of C−H bonds in the methyl group of *n*-butane and the methylene group of 1-butene, the rate-limiting step for the dehydrogenation of both compounds to 1-butene and 1,3-BD, respectively, relative to that for the reactions occurring over isolated Co sites. In summary, we have shown that Co−O−Zn sites in CoZn-DeAlBEA achieve high activity and selectivity for direct dehydrogenation of *n*-butane to 1,3-BD comparable to that reported for Pt-based catalysts but with the advantage of a much lower cost. This work demonstrates a promising strategy for *n*-butane dehydrogenation to 1,3-BD achieved by constructing non-noble bimetallic active sites in a zeolite framework.

■ ASSOCIATED CONTENT

Supporting Information

The Supporting Information is available free of charge at https://pubs.acs.org/doi/10.1021/jacs.5c16367.

Experimental section; supplemental catalyst characterization results (Figures S1−S9, Figure S14, Tables S3, S4); supplementary note for XPS analysis; supplementary note for Mears criterion analysis of external mass transport limitations and parameters (Tables S1, S2); supplemental reaction results (Figures S10−S13, S15−S21, Tables S6−S9); summary of non-noble-metal-based catalysts for *n*-butane dehydrogenation reported previously (Table S5); supplementary references (PDF)

■ AUTHOR INFORMATION

Corresponding Authors

Yanfei Zhang − *Joint R&D Center for Sustainable Marine Fuels, College of Environmental Science and Engineering, Dalian Maritime University, Dalian 116026, China; National Engineering Research Center of Lower-Carbon Catalysis Technology, Dalian Institute of Chemical Physics, Chinese Academy of Sciences, Dalian 116023, China;* orcid.org/0009-0003-3812-5642; Email: yfzh920@dlmu.edu.cn

Mingbin Gao − *State Key Laboratory of Physical Chemistry of Solid Surfaces, College of Chemistry and Chemical Engineering, Xiamen University, Xiamen 361005, China;* orcid.org/0000-0002-7143-2658; Email: mbgao@xmu.edu.cn

Alexis T. Bell − *Department of Chemical and Biomolecular Engineering, University of California, Berkeley, Berkeley, California 94720, United States;* orcid.org/0000-0002-5738-4645; Email: alexbell@berkeley.edu

Peng Tian − *National Engineering Research Center of Lower-Carbon Catalysis Technology, Dalian Institute of Chemical Physics, Chinese Academy of Sciences, Dalian 116023, China;* orcid.org/0000-0002-8768-0154; Email: tianpeng@dicp.ac.cn

Authors

Tingshu Yang − *Joint R&D Center for Sustainable Marine Fuels, College of Environmental Science and Engineering, Dalian Maritime University, Dalian 116026, China; National Engineering Research Center of Lower-Carbon Catalysis Technology, Dalian Institute of Chemical Physics, Chinese Academy of Sciences, Dalian 116023, China*

Jiaochan Hu − *Joint R&D Center for Sustainable Marine Fuels, College of Environmental Science and Engineering, Dalian Maritime University, Dalian 116026, China*

Linying Wang − *National Engineering Research Center of Lower-Carbon Catalysis Technology, Dalian Institute of Chemical Physics, Chinese Academy of Sciences, Dalian 116023, China*

Liang Qi − *National Engineering Research Center of Lower-Carbon Catalysis Technology, Dalian Institute of Chemical Physics, Chinese Academy of Sciences, Dalian 116023, China;* orcid.org/0000-0002-2155-2061

Zhongmin Liu − *National Engineering Research Center of Lower-Carbon Catalysis Technology, Dalian Institute of Chemical Physics, Chinese Academy of Sciences, Dalian 116023, China*

Complete contact information is available at: https://pubs.acs.org/10.1021/jacs.5c16367

Notes

The authors declare no competing financial interest.

■ ACKNOWLEDGMENTS

This work is supported by National Key Research and Development Program of China (2024YFE0207000), the National Natural Science Foundation of China (22302025, 22472173, 22288101, 22272171, and 22208337), and the Fundamental Research Funds for the Central Universities of Dalian Maritime University in China (3132023520). L. Q. also acknowledges the Youth Innovation Promotion Association, the Chinese Academy of Sciences (2023193). Y. Z. also acknowledges the Liaoning Province Doctoral Research Initiation Fund (2025-BS-0238).

■ REFERENCES

(1) Chu, M.; Liu, Y.; Gong, J.; et al. Suppressing dehydroisomerization boosts n-butane dehydrogenation with high butadiene selectivity. *Chem.—Eur. J.* **2021**, *27*, 11643−11648.

(2) Makshina, E. V.; Dusselier, M.; Janssens, W.; et al. Review of old chemistry and new catalytic advances in the on-purpose synthesis of butadiene. *Chem. Soc. Rev.* **2014**, *43*, 7917−7953.
(3) White, W. C. Butadiene production process overview. *Chem. Biol. Interact.* **2007**, *166*, 10−14.
(4) Wang, P.; Zhang, X.; Shi, R.; et al. Photocatalytic ethylene production by oxidative dehydrogenation of ethane with dioxygen on ZnO-supported PdZn intermetallic nanoparticles. *Nat. Commun.* **2024**, *15*, 789.
(5) Zheng, Y.; Li, J.; Zhang, X.; et al. Evolution of Co species in CO_2-assisted ethane dehydrogenation: Competing cleavage of C-H and C-C bonds. *ACS Catal.* **2024**, *14*, 4749−4759.
(6) Zhang, L.; Han, B.; Wang, B.; et al. Unraveling the roles of the ZnO surface structure and second metal doping in tuning the catalytic performance of ethane dehydrogenation. *ACS Catal.* **2025**, *15*, 5014−5027.
(7) Yu, X.; Li, G.; Tao, S.; et al. Single-atom Fe catalyst for catalytic ethane dehydrogenation to ethylene. *ChemCatChem.* **2023**, *15*, No. e202201612.
(8) Sattler, J. J. H. B.; Ruiz-Martinez, J.; Santillan-Jimenez, E.; et al. Catalytic dehydrogenation of light alkanes on metals and metal oxides. *Chem. Rev.* **2014**, *114*, 10613−10653.
(9) Bhasin, M. M.; Mccain, J. H.; Vora, B. V.; et al. Dehydrogenation and oxydehydrogenation of paraffins to olefins. *Appl. Catal. A-Gen.* **2001**, *221*, 397−419.
(10) Chen, S.; Xu, Y.; Chang, X.; et al. Defective $TiO_{(x)}$ overlayers catalyze propane dehydrogenation promoted by base metals. *Science* **2024**, *385*, 295−300.
(11) Camacho-Bunquin, J.; Ferrandon, M. S.; Sohn, H.; et al. Atomically precise strategy to a PtZn alloy nanocluster catalyst for the deep dehydrogenation of n-butane to 1,3-butadiene. *ACS Catal.* **2018**, *8*, 10058−10063.
(12) Chen, X.; Wang, M.; Ma, D.; et al. A highly efficient and regenerable Ir_1-Cu_1 dual-atom catalyst for low-temperature alkane dehydrogenation. *Nat. Catal.* **2025**, *8*, 436−447.
(13) Ajayi, B. P.; Jermy, B. R.; Ogunronbi, K. E.; et al. n-Butane dehydrogenation over mono and bimetallic MCM-41 catalysts under oxygen free atmosphere. *Catal. Today* **2013**, *204*, 189−196.
(14) Chen, C.; Hu, Z.; Ren, J.; et al. ZnO nanoclusters supported on dealuminated zeolite β as a novel catalyst for direct dehydrogenation of propane to propylene. *ChemCatChem.* **2019**, *11*, 868−877.
(15) Zhao, D.; Guo, K.; Han, S.; et al. Controlling reaction-induced loss of active sites in ZnO_x/Silicalite-1 for durable nonoxidative propane dehydrogenation. *ACS Catal.* **2022**, *12*, 4608−4617.
(16) Song, S. J.; Yang, K.; Zhang, P.; et al. Silicalite-1 stabilizes Zn-hydride species for efficient propane dehydrogenation. *ACS Catal.* **2022**, *12*, 5997−6006.
(17) Alghannam, A.; Bell, A. T. Effects of cofeeding hydrogen on propane dehydrogenation catalyzed by isolated iron sites incorporated into dealuminated BEA. *J. Am. Chem. Soc.* **2025**, *147*, 1677−1693.
(18) Dai, Y.; Gu, J.; Tian, S.; et al. γ-Al_2O_3 sheet-stabilized isolate Co^{2+} for catalytic propane dehydrogenation. *J. Catal.* **2020**, *381*, 482−492.
(19) Qu, Z. Q.; He, G. Y.; Zhang, T. J.; et al. Tricoordinated single-atom cobalt in zeolite boosting propane dehydrogenation. *J. Am. Chem. Soc.* **2024**, *146*, 8939−8948.
(20) Chen, C.; Zhang, S. M.; Wang, Z.; et al. Ultrasmall Co confined in the silanols of dealuminated beta zeolite: A highly active and selective catalyst for direct dehydrogenation of propane to propylene. *J. Catal.* **2020**, *383*, 77−87.
(21) Jaegers, N. R.; Danghyan, V.; Shangguan, J.; et al. Heterolytic C-H activation routes in catalytic dehydrogenation of light alkanes on Lewis acid-base pairs at ZrO_2 surfaces. *J. Am. Chem. Soc.* **2024**, *146*, 25710−25726.
(22) Chang, X.; Lu, Z.; Luo, R.; et al. Microenvironment engineering of non-noble metal alloy for selective propane dehydrogenation. *Chem.* **2025**, *11*, 102294.
(23) Zhang, X. B.; Liu, W.; Li, J. J.; et al. Dehydrogenation of n-butane on metal cobalt sites confined within ceria nanoislands. *ACS Catal.* **2024**, *14*, 15123−15132.
(24) Schweitzer, N. M.; Bo, Hu; Ujjal, D.; et al. Propylene hydrogenation and propane dehydrogenation by a single-site Zn^{2+} on silica catalyst. *ACS Catal.* **2014**, *4*, 1091−1098.
(25) Zhu, Q.; Wang, G.; Zhang, H.; et al. n-Butane dehydrogenation over Ni-Sn/SiO_2: Adsorption modes and reaction paths of n-butane and 1-butene. *Appl. Catal. A-Gen.* **2018**, *566*, 113−120.
(26) Chen, Y.; Zhao, J.; Gates, B. C.; et al. Stabilizing supported atom-precise low-nuclearity platinum cluster catalysts by nanoscale confinement. *Nat. Chem. Eng.* **2025**, *2*, 38−48.
(27) Alghannam, A.; Gates, B. C.; Bell, A. T.; et al. Unraveling the Unique Behavior of Atomically Dispersed Pt on Zeolite Fe-DeAlBEA for Catalyzing Propane Dehydrogenation with Cofed Hydrogen. *ACS Catal.* **2025**, *147*, 13784−13798.
(28) Zhang, B.; Song, M.; Xu, M.; et al. Recent advances in metal-zeolite catalysts for direct propane dehydrogenation. *Energy Fuels* **2023**, *37*, 19419−19432.
(29) Rodríguez, L.; Romero, D.; Rodríguez, D.; et al. Dehydrogenation of n-butane over Pd-Ga/Al_2O_3 catalysts. *Appl. Catal. A-Gen.* **2010**, *373*, 66−70.
(30) Nakaya, Y.; Furukawa, S. Tailoring single-atom platinum for selective and stable catalysts in propane dehydrogenation. *ChemPlusChem.* **2022**, *87*, No. e202100560.
(31) Wang, N.; Sun, Q. M.; Yu, J. H. Ultrasmall metal nanoparticles confined within crystalline nanoporous materials: A fascinating class of nanocatalysts. *Adv. Mater.* **2019**, *31*, 1803966.
(32) Chen, X. W.; Qin, X. T.; Jiao, Y. Y.; et al. Structure-dependence and metal-dependence on atomically dispersed Ir catalysts for efficient n-butane dehydrogenation. *Nat. Commun.* **2023**, *14*, 2588.
(33) Li, J.; Zhang, Q.; He, G.; et al. Silanol-stabilized atomically dispersed $Pt^{\delta+}$-O_x-Sn active sites in protozeolite for propane dehydrogenation. *J. Am. Chem. Soc.* **2024**, *146*, 24358−24367.
(34) Zhang, Y.; Qi, L.; Leonhardt, B.; et al. Mechanism and kinetics of n-butane dehydrogenation to 1,3-butadiene catalyzed by isolated Pt sites grafted onto ≡SiOZn-OH nests in dealuminated zeolite beta. *ACS Catal.* **2022**, *12*, 3333−3345.
(35) Qi, L.; Zhang, Y.; Babucci, M.; et al. Dehydrogenation of propane and n-butane catalyzed by isolated $PtZn_4$ sites supported on self-pillared zeolite pentasil nanosheets. *ACS Catal.* **2022**, *12*, 11177−11189.
(36) Qi, L.; Babucci, M.; Zhang, Y.; et al. Propane dehydrogenation catalyzed by isolated Pt atoms in ≡SiOZn-OH Nests in dealuminated zeolite beta. *J. Am. Chem. Soc.* **2021**, *143*, 21364−21378.
(37) Zhang, Y.; Qi, L.; Nozik, D.; et al. Mechanism and kinetics of propane and n-butane dehydrogenation over isolated and nested ≡SiOZn-OH sites grafted onto silanol nests of dealuminated beta zeolite. *ACS Catal.* **2024**, *14*, 2787−2804.
(38) Medeiros-Costa, I. C.; Dib, E.; Mintova, S.; et al. Silanol defect engineering and healing in zeolites: opportunities to fine-tune their properties and performances. *Chem. Soc. Rev.* **2021**, *50*, 11156−11179.
(39) Johnson, B. A.; Di Iorio, J. R.; Roman-Leshkov, Y. Identification and quantification of distinct active sites in Hf-Beta zeolites for transfer hydrogenation catalysis. *J. Catal.* **2021**, *404*, 607−619.
(40) Qi, L.; Das, S.; Zhang, Y.; et al. Ethene hydroformylation catalyzed by rhodium dispersed with zinc or cobalt in silanol nests of dealuminated zeolite Beta. *J. Am. Chem. Soc.* **2023**, *145*, 2911−2929.
(41) Hu, Z. P.; Qin, G. Q.; Han, J. F.; et al. Atomic insight into the local structure and microenvironment of isolated Co-motifs in MFI zeolite frameworks for propane dehydrogenation. *J. Am. Chem. Soc.* **2022**, *144*, 12127−12137.
(42) Chai, Y. C.; Chen, S. H.; Chen, Y.; et al. Dual-atom catalyst with N-colligated Zn Co species as dominant active sites for propane dehydrogenation. *J. Am. Chem. Soc.* **2024**, *146*, 263−273.
(43) Qi, L.; Zhang, Y. F.; Conrad, M. A.; et al. Ethanol conversion to butadiene over isolated zinc and yttrium sites grafted onto

dealuminated beta zeolite. *J. Am. Chem. Soc.* **2020**, *142*, 14674−14687.
(44) Chupin, C.; Van Veen, A. C.; Konduru, M.; et al. Identity and location of active species for NO reduction by CH_4 over Co-ZSM-5. *J. Catal.* **2006**, *241*, 103−114.
(45) Martínez-Hernández, A.; Fuentes, G. A. Redistribution of cobalt species in Co-ZSM5 during operation under wet conditions in the reduction of NO_x by propane. *Appl. Catal., B* **2005**, *57*, 167−174.
(46) Dzwigaj, S.; Che, M. Incorporation of Co(II) in dealuminated BEA zeolite at lattice tetrahedral sites evidenced by XRD, FTIR, diffuse reflectance UV-Vis, EPR, and TPR. *J. Phys. Chem. B* **2006**, *110*, 12490−12493.
(47) Janas, J.; Shishido, T.; Che, M.; et al. Role of tetrahedral Co(II) sites of CoSiBEA zeolite in the selective catalytic reduction of NO: XRD, UV-vis, XAS and catalysis study. *Appl. Catal., B* **2009**, *89*, 196−203.
(48) Nozik, D.; Tinga, F. M. P.; Bell, A. T. Propane dehydrogenation and cracking over Zn/H-MFI prepared by solid-state ion exchange of $ZnCl_2$. *ACS Catal.* **2021**, *11*, 14489−14506.
(49) Kopač, D.; Jurković, D. L.; Likozar, B.; et al. First-principles-based multiscale modelling of nonoxidative butane dehydrogenation on Cr_2O_3(0001). *ACS Catal.* **2020**, *10*, 14732−14746.
(50) Huang, Y.-A.; Cheng, G.; Lei, M.; et al. Decoding the kinetic complexity of Pt-catalyzed n-butane dehydrogenation by machine learning and microkinetic analysis. *ACS Catal.* **2024**, *14*, 7978−7995.
(51) Hauser, A. W., Gomes, J., Bajdich, M., et al. Subnanometer-sized Pt/Sn alloy cluster catalysts for the dehydrogenation of linear alkanes. *Phys. Chem. Chem. Phys. 15*, (**2013**), 20727.
(52) Wang, J.; Hokkanen, B.; Burghaus, U. Adsorption of iso-butane on ZnO(0001)-Zn. *Surf. Sci.* **2006**, *600*, 4855−4859.
(53) Zeng, T.; Sun, G.; Miao, C.; et al. Stabilizing oxidative dehydrogenation active sites at high temperature with steam: $ZnFe_2O_4$-catalyzed oxidative dehydrogenation of 1-butene to 1,3-butadiene. *ACS Catal.* **2020**, *10*, 12888−12897.

https://doi.org/10.1021/jacs.5c16367
J. Am. Chem. Soc. 2025, 147, 42110−42122